Numerical Study of Gas-Particle Flow in a Solid Rocket Nozzle

C. J. Hwang*
National Cheng Kung University, Taiwan, Republic of China
and
G. C. Chang†
Chung Shan Institute of Science and Technology, Taiwan, Republic of China

The numerical solution procedure has been developed to analyze gas-particle flow in a solid rocket nozzle. The time-dependent, explicit MacCormack scheme is adopted to solve the governing equations derived from the trajectory model. The velocity, trajectory, and temperature of the solid particles are treated with the Lagrangian approach. To study the particle diffusive velocity, which is included to account for the turbulent effect, the equation of particle number density is solved by the hybrid scheme. The results of this study indicate the level of gas-particle coupling and the differences that can be expected for the different sizes and mass fractions of particles.

Nomenclature

a = sound speed based on the temperature of gas phase, $\sqrt{\gamma RT}$
C_D = drag coefficient
C_p = specific heat at constant pressure, 1.067 [KJ/(Kg − K)]
C_μ = constant in Eq. (14), 0.09
D_p = diameter of particle
e = turbulence dissipation rate
H = enthalpy
k = conductivity
$\dot{m}_j$ = particle mass flow rate at jth location on the inlet plane
m_p = mass per particle, $[m_p/(1/6)\pi D_p^3] = 4004.8$ (Kg/m^3)
M = Mach number, $[(|V|)/a]$
M_p = $[(|V - V_p|)/a]$
NPS = number of trajectories of particles
Nu_p = Nusselt number
n_p = number density of particle
P = pressure
Pr = Prandtl number, 0.74
P_T = total pressure, 1.034×10^6 (N/m^2)
q = turbulence energy
R = gas constant, 287.07×10^{-3} [KJ/(Kg − K)]
Re_p = $[(\rho|V - V_p|D_p)/\mu_M]$
r = radius of particle, 1, 5, 10, 20 (μm)
S_{pm} = mass source
S_{pu}, S_{pv} = momentum sources in x, y directions
S_{ph} = energy source
T = temperature
T_T = total temperature, 555.6 K
u, v = velocity components in x, y directions
V_{pc} = particle convective velocity
V_{pd} = particle diffusive velocity
V_{po} = initial particle velocity
X_{po} = particle position at the beginning of the time increment
x, y, t = physical coordinates
Y_{jk} = mass fraction of kth class of particle at jth location
μ = first viscosity coefficient, $\mu_o\,(T/T_T)^{0.6}$ [Kg/(m − s)]
μ_o = 2.68×10^{-5} [Kg/(m − s)]
λ = second viscosity coefficient
ϕ = particle mass fraction, 10, 20, 25, 30 (%)
Γ = turbulent diffusivity
σ = Schmidt number
σ_p^t = 1.0 − 2.0 (Ref. 20)
ν = kinematic viscosity
ρ = density
γ = ratio of specific heat, 1.4

Subscripts

M = molecular
p = particle
T = turbulent

Superscript

t = turbulent

Received April 16, 1987; presented as Paper 87-2168 at the AIAA/SAE/ASME/ASEE 23rd Joint Propulsion Conference, San Diego, CA, June 29-July 2, 1987; revision received Jan. 13, 1988.

*Associate Professor, Institute of Aeronautics and Astronautics.
†Assistant Scientist, Jet Propulsion Center.

Introduction

THERE are many problems that require the numerical solution of compressible two-phase flow in nozzles. One example of an important problem is the exhaust gas from a solid propellant rocket motor. The aluminum oxide particles in the exhaust contribute to an inefficiency in the expansion process in the propulsive nozzle. The inefficiency is due to the nonequilibrium effects, primarily velocity and thermal lags between the gas and particles. From the preceding discussion, it is necessary to know the behavior of the particle-laden gas expanding through the nozzle in order to predict, evaluate, or design solid rocket motor performance.

To understand previous research efforts on this topic, several research papers were studied. A comprehensive review of gas-particle nozzle flows before 1962 was presented by Hoglund.[1] This paper presented the two-phase flow theory and experimental studies and discussed the one-dimensional approximations. Kliegel[2] introduced the "constant lag" concept to calculate the coupled, one-dimensional gas-particle behavior for an inviscid gas. For the inviscid two-dimensional gas-particle flow, Kliegel and Nickerson[3] showed that the equations are hyperbolic and

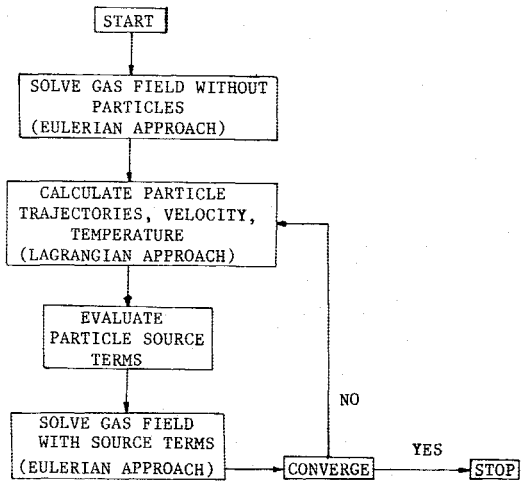

Fig. 1 Flow chart for trajectory model.

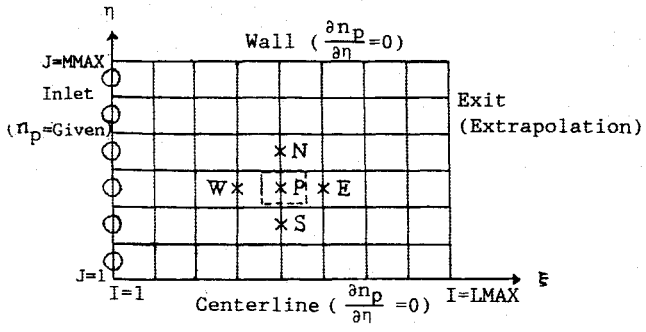

Fig. 2 Computational cell and boundary conditions for the number density of particles.

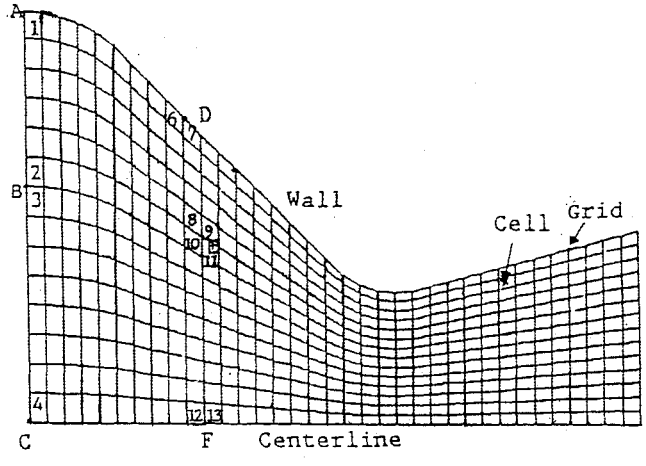

SPA = $\frac{1}{4}$ SP1 SPD = $\frac{1}{4}$ SP6 + $\frac{1}{4}$ SP7

SPB = $\frac{1}{4}$ (SP2 + SP3) SPE = $\frac{1}{4}$ (SP8+SP9+SP10+SP11)

SPC = $\frac{1}{2}$ SP4 SPF = $\frac{1}{2}$ (SP12 + SP13)

* SPK : source terms at grid point K (A,B,C,D,E,F)

SPH : source terms at cell H (1-13)

Fig. 3 Numerical treatment for the source terms on the grids.

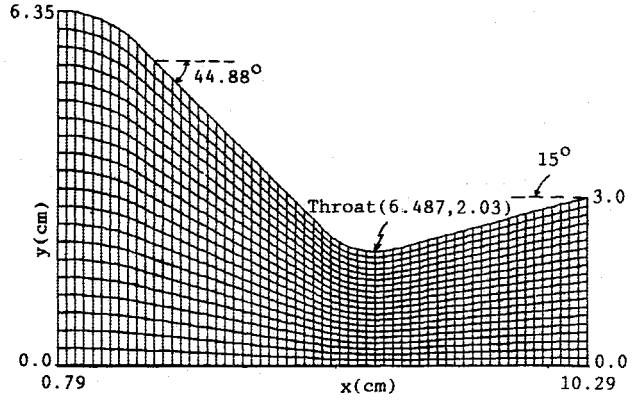

Fig. 4 Grid for conical nozzle (61 × 21).

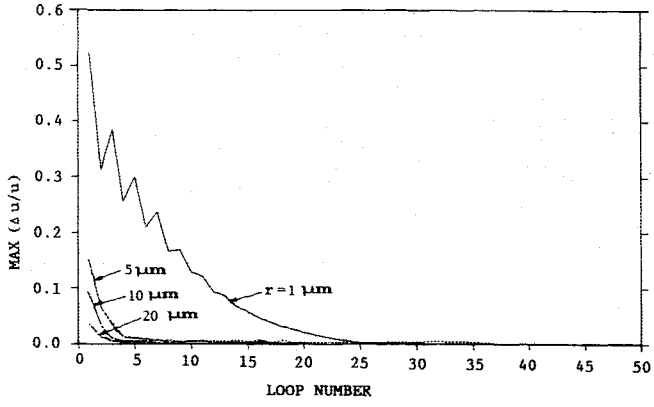

Fig. 5 Convergent history for inviscid gas-particle flow.

can be solved by the method of characteristic in the supersonic region of nozzle. A complete review of numerical models for dilute gas-particle flows has been presented by Crowe.[4] The models can be categorized according to coupling, dimension, and approach. The advantages and disadvantages of two-fluid and trajectory models are also discussed. In recent years, numerical methods have been broadly applied to the complicated sets of governing equations. Nickerson,[5] Chang,[6] Hwang,[7] and DiGiacinto[8] have used a two-fluid model to solve for dilute gas-particle flows. As mentioned in Ref. 4, the numerical instabilities, numerical diffusion, and large storage requirements for multiple particle sizes are inherent difficulties in the two-fluid model. The trajectory model can be thought of as the "natural" solution scheme, and storage requirements for multiple particle sizes are not excessive. Crowe[9] and Dukowicz[10] have applied the trajectory model to solve the gas-droplet flows. The Euler approach was used in the gas flow, and the droplets were treated in a Lagrangian fashion.

The purpose of this study is to demonstrate a numerical procedure that can predict the physical properties and physical phenomena of gas-particle nozzle flow. Considering the works of previous authors, the trajectory model is employed. In this paper, the solid rocket nozzle flow is investigated. Different kinds of particle mass fractions and particle sizes are discussed. In order to simulate the particle dispersion, the model of Melville and Bray[11] is selected.

Mathematical Model

Governing Equations

In order to treat the gas-particle flow, the following set of governing equations, which includes the turbulent effect[12] and particle source terms (S_{pm}, S_{pu}, S_{pv}, S_{ph}), is employed. The nonconservative form is written and expressed in Eqs. (1-5):

$$\frac{\partial \rho}{\partial t} + u\frac{\partial \rho}{\partial x} + v\frac{\partial \rho}{\partial y} + \rho\left(\frac{\partial u}{\partial x} + \frac{\partial v}{\partial y} + \frac{v}{y}\right) = \left[\frac{\partial}{\partial x}\left(\frac{\mu_T}{\rho}\frac{\partial \rho}{\partial x}\right) + \frac{\partial}{\partial y}\left(\frac{\mu_T}{\rho}\frac{\partial \rho}{\partial y}\right) + \left(\frac{\mu_T}{\rho y}\frac{\partial \rho}{\partial y}\right)\right] + S_{pm} \tag{1}$$

$$\frac{\partial u}{\partial t} + u\frac{\partial u}{\partial x} + v\frac{\partial u}{\partial y} + \frac{1}{\rho}\frac{\partial P}{\partial x} = \frac{1}{\rho}\frac{\partial}{\partial x}\left[(\lambda + 2\mu)\frac{\partial u}{\partial x} + \lambda\frac{\partial v}{\partial y}\right] + \frac{1}{\rho}\frac{\partial}{\partial y}\left[\mu\left(\frac{\partial v}{\partial x} + \frac{\partial u}{\partial y}\right)\right] + \frac{1}{\rho}\left[u\frac{\partial}{\partial x}\left(\frac{\mu_T}{\rho}\frac{\partial \rho}{\partial x}\right) + v\frac{\partial}{\partial y}\left(\frac{\mu_T}{\rho}\frac{\partial \rho}{\partial x}\right)\right] + \frac{1}{\rho y}\left[(\lambda + \mu)\frac{\partial v}{\partial x} + \mu\frac{\partial u}{\partial y} + \frac{\mu_T v}{\rho}\frac{\partial \rho}{\partial x}\right] - \frac{1}{\rho}\frac{2}{3}\frac{\partial \rho q}{\partial x} + \frac{S_{pu}}{\rho} \tag{2}$$

$$\frac{\partial v}{\partial t} + u\frac{\partial v}{\partial x} + v\frac{\partial v}{\partial y} + \frac{1}{\rho}\frac{\partial P}{\partial y} = \frac{1}{\rho}\frac{\partial}{\partial y}\left[(\lambda + 2\mu)\frac{\partial v}{\partial y} + \lambda\frac{\partial u}{\partial x}\right] + \frac{1}{\rho}\frac{\partial}{\partial x}\left[\mu\left(\frac{\partial v}{\partial x} + \frac{\partial u}{\partial y}\right)\right] + \frac{1}{\rho}\left[v\frac{\partial}{\partial y}\left(\frac{\mu_T}{\rho}\frac{\partial \rho}{\partial y}\right) + u\frac{\partial}{\partial x}\left(\frac{\mu_T}{\rho}\frac{\partial \rho}{\partial y}\right)\right] + \frac{1}{\rho y}\left[(\lambda + 2\mu) \times \left(\frac{\partial v}{\partial y} - \frac{v}{y}\right) + \frac{\mu_T v}{\rho}\frac{\partial \rho}{\partial y}\right] - \frac{1}{\rho}\frac{2}{3}\frac{\partial \rho q}{\partial y} + \frac{S_{pv}}{\rho} \tag{3}$$

$$\frac{\partial P}{\partial t} + u\frac{\partial P}{\partial x} + v\frac{\partial P}{\partial y} - a^2\left(\frac{\partial \rho}{\partial t} + u\frac{\partial \rho}{\partial x} + v\frac{\partial \rho}{\partial y}\right) = (\gamma - 1)\left\{(\lambda_M + 2\mu_M)\left[\left(\frac{\partial u}{\partial x}\right)^2 + \left(\frac{\partial v}{\partial y}\right)^2\right] + \mu_M\left[\left(\frac{\partial v}{\partial x}\right)^2 + \left(\frac{\partial u}{\partial y}\right)^2\right] + 2\lambda_M\frac{\partial u}{\partial x}\frac{\partial v}{\partial y} + 2\mu_M\frac{\partial v}{\partial x}\frac{\partial u}{\partial y} + \frac{\partial}{\partial x}\left(k\frac{\partial T}{\partial x}\right) + \frac{\partial}{\partial y}\left(k\frac{\partial T}{\partial y}\right) - RT\left[\frac{\partial}{\partial x}\left(\frac{\mu_T}{\rho}\frac{\partial \rho}{\partial x}\right) + \frac{\partial}{\partial y}\left(\frac{\mu_T}{\rho}\frac{\partial \rho}{\partial y}\right)\right] + \frac{1}{y}\left[(\lambda_M + 2\mu_M)\frac{v^2}{y} + 2\lambda_M v\left(\frac{\partial u}{\partial x} + \frac{\partial v}{\partial y}\right) + k\frac{\partial T}{\partial y} - \frac{\mu_T RT}{\rho}\frac{\partial \rho}{\partial y}\right] + \rho e + 2\mu\left(\frac{\partial q^{1/2}}{\partial x} + \frac{\partial q^{1/2}}{\partial y}\right)^2 + S_{ph}\right\} \tag{4}$$

$$P = \rho RT \tag{5}$$

In the present work, the Jones-Launder[13] turbulence model is employed. The mathematical forms for the turbulence energy q and turbulence dissipation rate e are the same as those of Ref. 12. For the future study of two-phase turbulent flow, the two-equation model with inclusion of generation and dissipation of turbulent energy by the relative motion, such as that given in Ref. 14, is suggested.

For the trajectory model, particles are tracked through the flowfield. The particle momentum and heat-transfer equations can be integrated using the Lagrangian approach to obtain the velocity, position, and temperature. The net difference of particle properties between entering and leaving a given cell provides the particle source terms, which can be calculated from the following equations:

Mass source term:

$$S_{pm} = \sum_{i=1}^{\text{NPS}}\left[(\dot{m}_p)_{\text{in cell}} - (\dot{m}_p)_{\text{out cell}}\right]_i \tag{6}$$

where

$$\dot{m}_p = \dot{m}_j Y_{jk} \tag{7}$$

Momentum source term:

$$S_{pu} = \sum_{i=1}^{\text{NPS}}\left[(\dot{m}_p u_p)_{\text{in cell}} - (\dot{m}_p u_p)_{\text{out cell}}\right]_i \tag{8}$$

$$S_{pv} = \sum_{i=1}^{\text{NPS}}\left[(\dot{m}_p v_p)_{\text{in cell}} - (\dot{m}_p v_p)_{\text{out cell}}\right]_i \tag{9}$$

where

$$m_p\frac{\mathrm{d}(V_{pc})}{\mathrm{d}t} = \frac{\pi D_p^2 \rho C_D}{8}|V - V_p|(V - V_p) \tag{10}$$

$$V_{pd}n_p = -\Gamma_p \nabla n_p \tag{11}$$

and

$$V_p = V_{pc} + V_{pd} \tag{12}$$

The particle diffusivity Γ_p and particle number density n_p, which are described in Ref. 15, are calculated from the following relations:

$$\Gamma_p = \frac{\nu_p^t}{\sigma_p^t} \tag{13}$$

$$\nu_p^t = \nu^t\left[1 + \left(\frac{[(m_p)/(3\pi\mu_M D_p)]}{1.5C_\mu q/e}\right)\right]^{-1} \tag{14}$$

$$\frac{\partial}{\partial x}(un_p) + \frac{1}{y}\frac{\partial}{\partial y}(y\,vn_p) - \frac{\partial}{\partial x}\left(\Gamma_p\frac{\partial n_p}{\partial x}\right) - \frac{1}{y}\frac{\partial}{\partial y}\left(y\Gamma_p\frac{\partial n_p}{\partial y}\right) = 0 \tag{15}$$

Energy source term:

$$S_{ph} = \sum_{i=1}^{\text{NPS}}\left[(\dot{m}_p H_p)_{\text{in cell}} - (\dot{m}_p H_p)_{\text{out cell}}\right]_i \tag{16}$$

where

$$m_p\frac{\mathrm{d}H_p}{\mathrm{d}t} = Nu_p\pi k D_p(T - T_p) \tag{17}$$

For the general cases of two-phase flow, the energy source term should contain the work done by the interphase forces,[7] which appears as kinetic energy terms in Eq. (16). The temperature of particles can be calculated from the following relation:[16]

$$H_p = aT_p + \tfrac{1}{2}(b \times 10^{-3})T_p^2 + \tfrac{1}{3}(c \times 10^{-6})T_p^3 - \frac{d \times 10^5}{T_p} - A + (H_p)_{298\text{ K}} \tag{18}$$

where a, b, c, d, and A are constants that depend on the materials of particles.

Drag Coefficient and Nusselt Number

Two important relations that show the interaction between the gas phase and particle phase are drag coefficient and Nusselt number. From the discussion of Nickerson,[5] the fol-

lowing form of drag coefficient is employed in this study:

$$C_D = (C_{Do} - 2)\exp\left[-3.07\sqrt{\gamma}\,\frac{M_p}{Re_p}\,g(Re_p)\right] + \frac{h(M_p)}{\sqrt{\gamma}M_p}\exp\left(-\frac{Re_p}{2M_p}\right) + 2 \tag{19}$$

where

$$g(Re_p) = \frac{1 + Re_p(12.278 + 0.584Re_p)}{1 + 11.278Re_p}, \quad Re_p < 10^3 \tag{20}$$

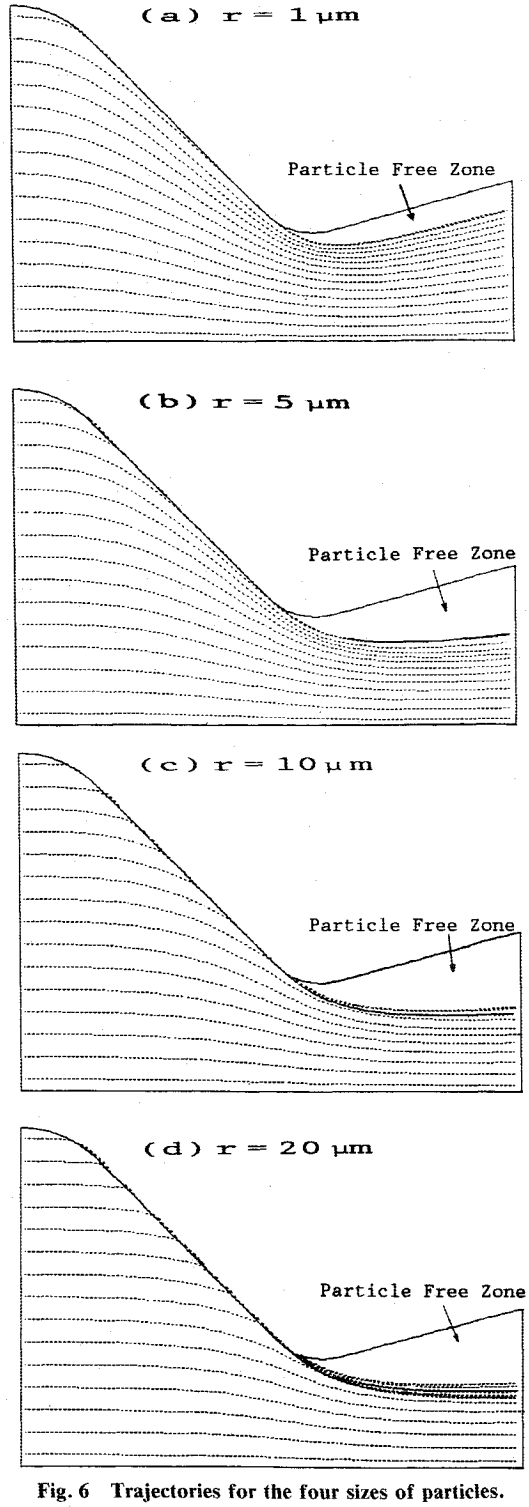

Fig. 6 Trajectories for the four sizes of particles.

$$h(M_p) = [(5.6)/(M_p + 1)] + 1.7\sqrt{(T_p/T)} \tag{21}$$

$$C_{Do} = \begin{cases} 24/Re_p, & 0 < Re_p \le 0.34 \\ 0.48 + 28Re_p^{-0.85}, & 0.34 < Re_p \le 10^5 \end{cases} \tag{22}$$

In the present work, the Nusselt number proposed by Drake-Kavanaugh[17] is used to study the heat transfer between gas and particle phases. The mathematical form of Nu_p is given here:

$$Nu_p = \frac{Nu_{po}}{1 + 3.42\,[(M_p)/(Re_pPr)]\,Nu_{po}} \tag{23}$$

where

$$Nu_{po} = 2.0 + 0.6\,Re_p^{0.5}\,Pr^{0.33} \tag{24}$$

Numerical Approach

As mentioned before, the trajectory model is applied to solve the gas-particle flow problems. The solution procedure of this work is shown in Fig. 1. The numerical treatments for the gas and particle phases are given in the following descriptions.

Gas Phase

By using the typical coordinate transformation,[12] the MacCormack scheme[18] was applied to solve Eqs. (1–5). At the centerline, l'Hospital's rule with symmetric considerations and a one-sided difference are used. Because the entrance flow is subsonic in this work, the total pressure, total temperature, and flow angle are given. The reference-plane-characteristic scheme is introduced. For the supersonic outflow, the properties at the exit plane are calculated by the space extrapolation from upstream interior points. In the present study, the nozzle wall is assumed to be impermeable and adiabatic. The slip and no-slip conditions for the inviscid and viscous flows are considered. As in the treatment of inlet, the reference-plane-characteristic scheme is employed. In order to overcome numerical oscillation problems and accelerate the convergence, the artificial viscosity, time smoothing, and subcycle techniques are suggested. The details of the preceding discussions are given in Ref. 12.

Particle Phase

At the inlet plane, the positions of particles are equally distributed by the number of trajectories. The temperature and velocity of the particle phase are same as those of the gas phase. The number density of particles is decided by the particle mass fraction, mass flow rate, and number of trajectories. After obtaining the number density distribution at the nozzle inlet, the boundary conditions and computational cell with hybrid scheme,[19] which are shown in Fig. 2, are employed to find the values of n_p from Eq. (15). By integrating Eq. (10) with time, the convective velocity of particle can be obtained by the following relation:

$$V_{pc} = V - (V - V_{po})\,e^{-(\Delta t/\tau)} \tag{25}$$

where

$$\tau = \frac{8m_p}{\pi D_p \mu_M C_D Re_p} \tag{26}$$

From Eqs. (11) and (12), the diffusive velocity and particle velocity are calculated. After determining the new particle velocity, the particle position is obtained from

$$X_p = X_{po} + (V_p + V_{po})\,[(\Delta t)/2] \tag{27}$$

From Eqs. (17) and (18), the particle temperature can be obtained. In the present solution procedure, Δt is decided by the grid space and particle velocity. For a given cell, the source terms are calculated according to Eqs. (6), (8), (9), and (16).

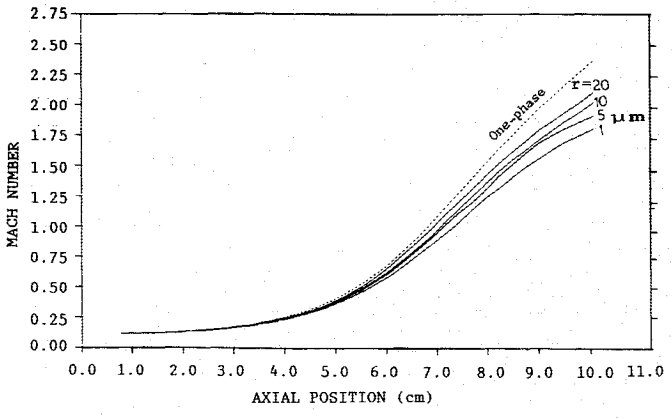

Fig. 7 Mach number distribution at the centerline.

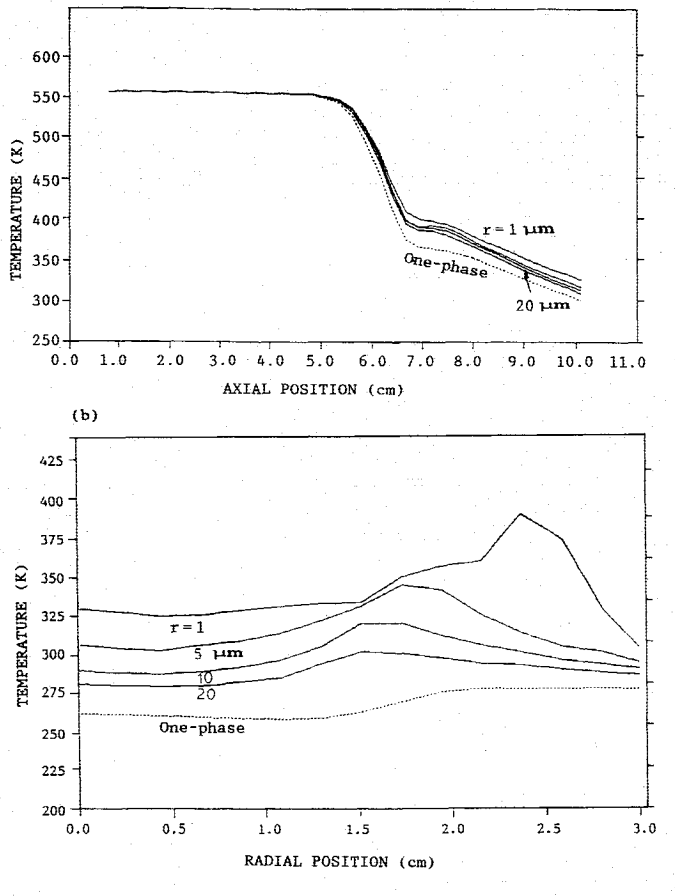

Fig. 8 Gas temperature distributions at the: a) nozzle wall; and b) exit plane.

Because the grid points do not locate inside the cells, the source terms at the grids are expressed by the average of surrounding values. The numerical treatment is shown in Fig. 3.

Results and Discussion

To study the physical phenomena, two-phase flows passing through the solid rocket nozzle, which is shown in Fig. 4, are investigated. The values of parameters are listed in the nomenclature.

Inviscid Gas-Particle Flow

Even though the gas is assumed to be inviscid, the drag force between the gas phase and the particle phase exists. The

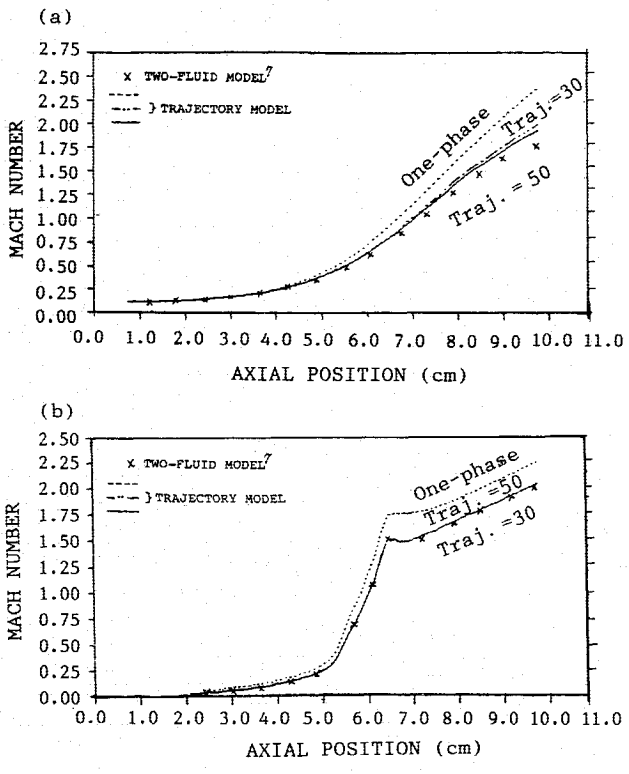

Fig. 9 Mach number distributions at the: a) centerline; and b) nozzle wall.

two-phase flows with 30% particle mass fraction and four kinds of particle sizes (1, 5, 10, and 20 μm) are considered. For the mesh with 36×15 grid points, the convergent history is studied, and the results are given in Fig. 5. The "Loop Number" represents the numbers of calculations for the source terms. For the different sizes of particles, the trajectories are plotted in Fig. 6. It is consistent with the fact that the particle-free zone for the small particle is smaller than that of the large particle. The small particles can more easily be parallel to the wall at the convergent part of the nozzle. From the Mach number and temperature distributions shown in Figs. 7 and 8, the differences between one-phase (clean gas) and two-phase flows are larger for the smaller particles. To validate the solution procedure, the numerical data given in Fig. 7 were compared with related data presented by Chang.[6] The similar profiles confirm that the present study is reliable. Due to the existence of a particle free zone, the temperature difference between one- and two-phase flows at the wall is smaller than that at the centerline. From the particle trajectories plotted in Fig. 6, it is easy to determine that the peak values of temperature appear around the limiting particle streamlines. These results are shown in Fig. 8b.

To further evaluate the accuracy of this work, the results are compared with those of Hwang.[7] The mesh given in Fig. 4 was used. Particles with 1 μm and 30% mass fraction were considered. For the different numbers of trajectories, 30 and 50, the Mach number distributions are given in Fig. 9. Along the nozzle wall, the solutions of trajectory and two-fluid models coincide exactly. Although the Mach numbers along the centerline don't match very well for those two models, the numerical difference becomes small when the number of trajectories is increased. In this paper, the total temperature is constant (555.6 K) and the wall is adiabatic. Because of these assumptions, the Mach number distributions given in Fig. 9b can be explained from the trend of temperature shown in Fig. 8a.

Until now, only one class of particle is considered for each case. To further study the physical phenomena, the exhaust gas, which includes the combination of three classes of particles—(1 μm, 7.5%), (5 μm, 15%), and (10 μm, 7.5%)—is

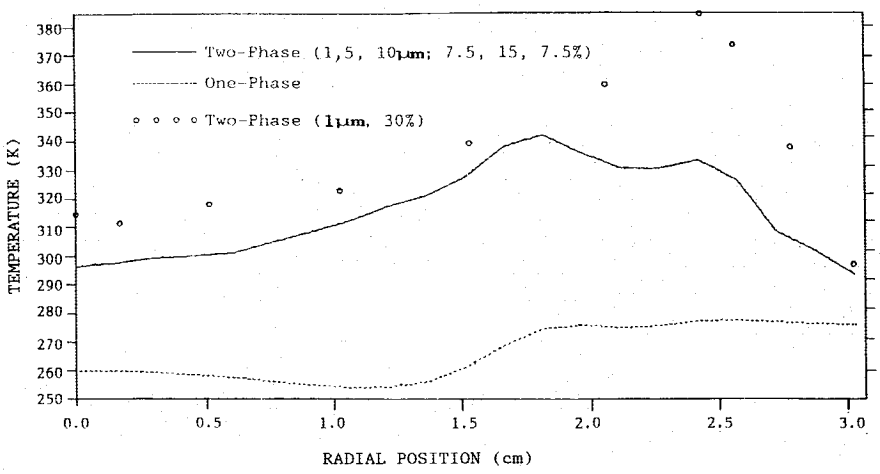

Fig. 10 Gas temperature distribution at the exit plane.

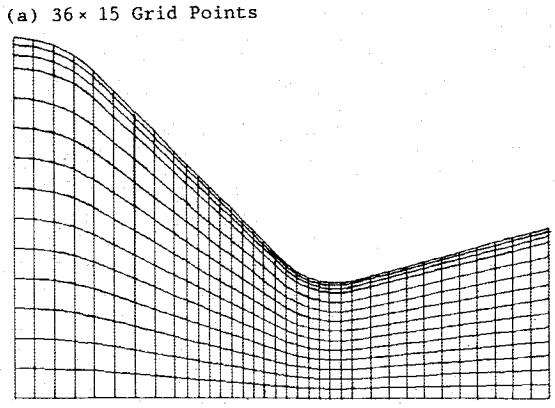

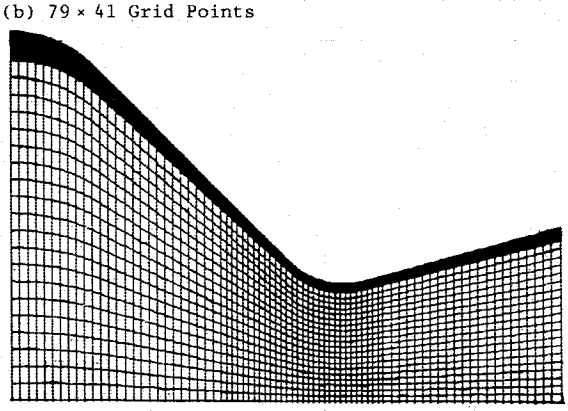

Fig. 11 Grid for conical nozzle.

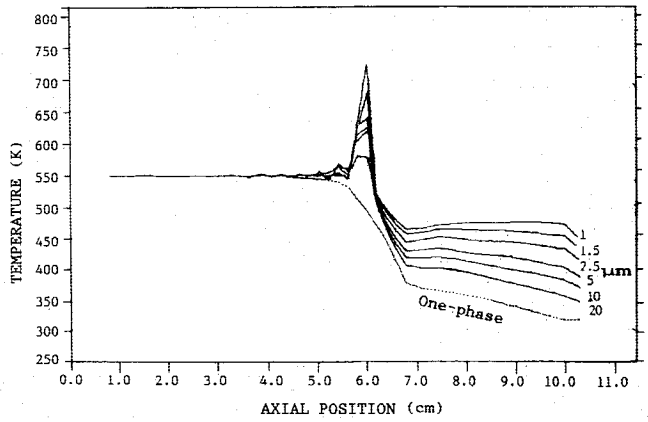

Fig. 13 Gas temperature distribution at the nozzle wall.

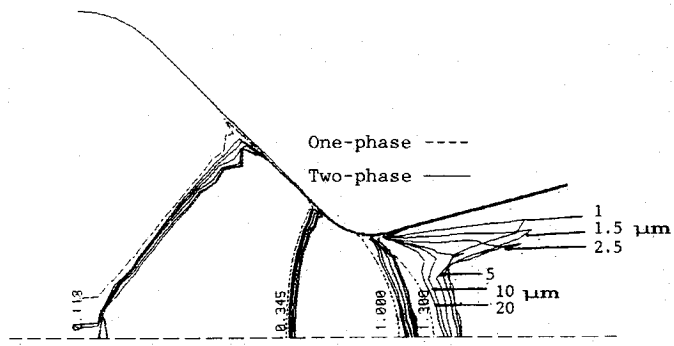

Fig. 14 Mach number contour for viscous gas-particle flow.

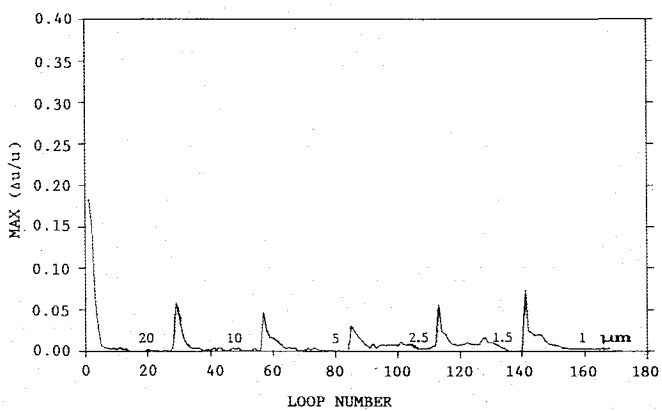

Fig. 12 Convergent procedure for the viscous gas-particle flow.

employed. In the present work, the interaction between particles is neglected. Due to this assumption and the results shown in Fig. 6, it is obvious that the particle free zone of two-phase flow with multiple sizes of particles is decided by the small particle, and the trajectories of particles become complicated. Because of this phenomenon, the irregular shape of temperature distribution given in Fig. 10 is observed, and two peak values occur. From the previous discussions and the data given in Fig. 8b, the temperature of two-phase flow with multiple sizes of particles should be lower than that of two-phase flow with one single small size of particle, if the total mass fraction is kept constant. This fact is shown in Fig. 10.

Viscous Gas-Particle Flow

To simulate the boundary layer and high gradient of properties in the throat region, the unequal grids shown in Fig.

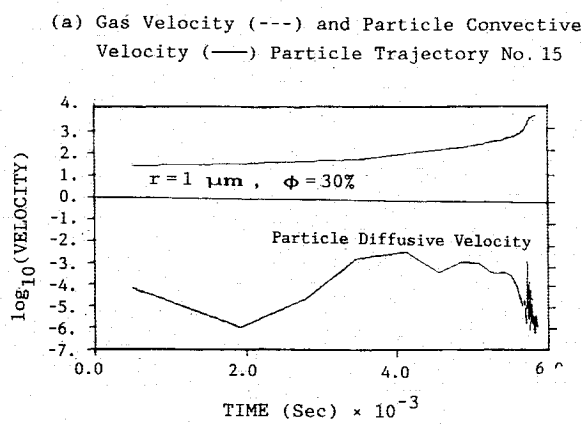

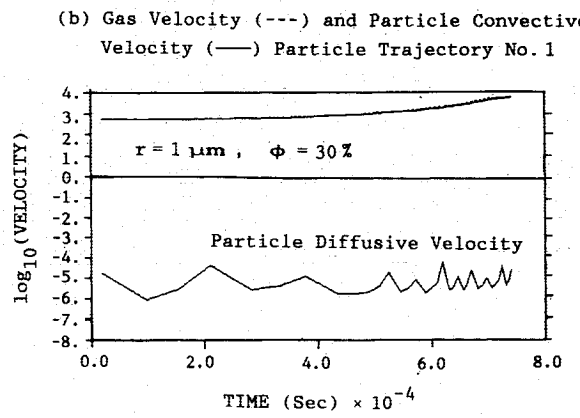

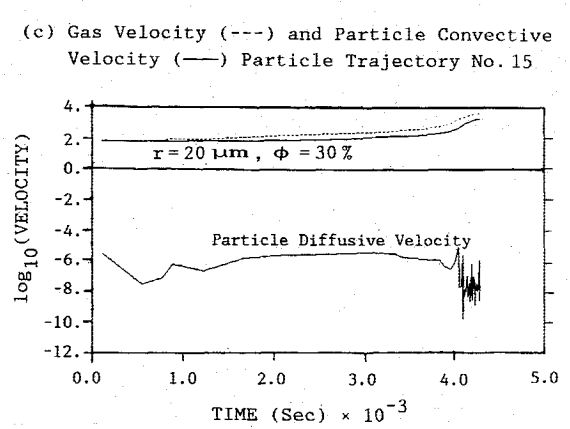

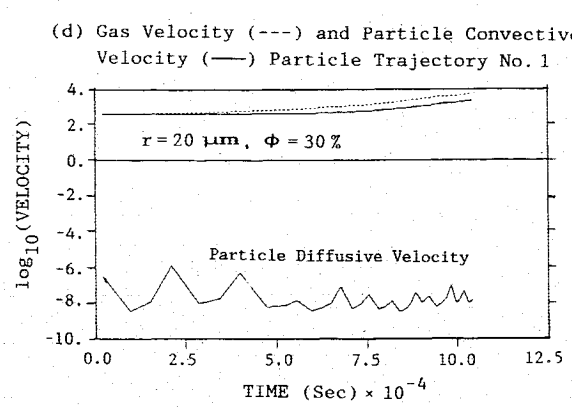

Fig. 15 Gas velocity, particle convective velocity, and particle diffusive velocity along two trajectories.

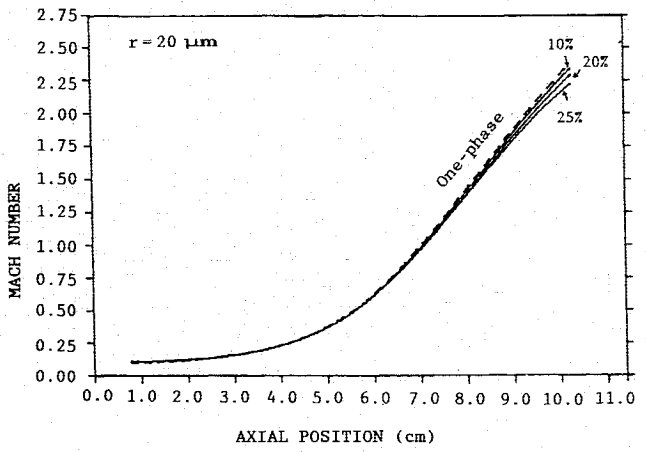

Fig. 16 Mach number distribution at the centerline.

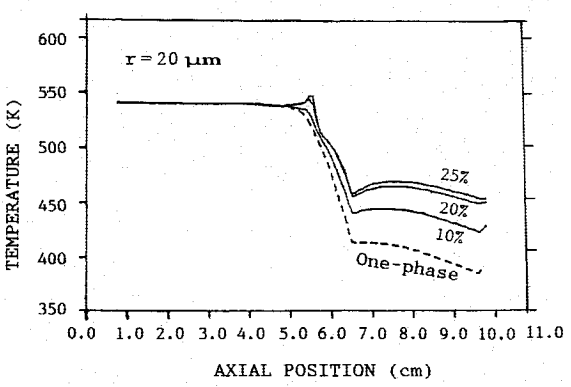

Fig. 17 Gas temperature distribution at the nozzle wall.

11 are employed. Two major studies, which include the effects of particle sizes and particle mass fractions on the turbulent gas-particle flow, are worked out in this topic. For the constant mass fraction (30%), the grid given in Fig. 11a is used to solve the two-phase flow with different sizes of particles. Because the convergence of solution for the particle with 1 μm is difficult, the following alternative way is introduced. Considering the result of one-phase flow to be the initial guess, convergence of solution for the large-particle (20 μm) flow can be achieved. The solution for the particle (10 μm) flow is obtained when the result of 20 μm particle flow is assumed to be the initial guess. In the same way, the numerical results for all sizes of particles can be obtained. The convergent procedure is shown in Fig. 12.

Under this solution procedure, the temperature distributions along the nozzle wall are plotted in Fig. 13. As in Fig. 8a, the gas temperature is higher for the two-phase flow with small sizes of particles; the peak values occur, however around the particle separation points. This phenomenon did not happen for the inviscid gas-particle flow or viscous one-phase flow. From the Mach number contour in Fig. 14, the sonic line moves farther downstream for the two-phase flow. When sizes of particles are increased, the peaks of profiles are shifted to the direction of centerline, and the magnitudes are decreased. The particle free zone can be used to explain this behavior. The observed fluctuations in the first contour near the wall may be caused by the discretization error due to the course grid shown in Fig. 11a. Even though the present turbulent model maybe not simulate the flowfield completely, it is worthwhile to study the diffusive velocity of particles. Along two trajectories, which are near the centerline (no. 1) and nozzle wall (no. 15), the magnitudes of velocities are investigated. As shown in Fig. 15, the difference between the gas velocity and the convective velocity of a particle of 1 μm is smaller than that for the 20 μm particle.

It is obvious that the order of magnitude for the convective velocity is larger than that for the diffusive velocity. The diffusive velocity is oscillatory with time, and the high frequency appears in the supersonic region.

To further investigate the flow behavior, the mesh shown in Fig. 11b is introduced. In this case, the radius of particles is 20 μm, and three kinds of mass fraction (10, 20, and 25%) are chosen. From the physical concept, the Mach number for the low mass fraction should be larger than that for the high mass fraction. The results shown in Fig. 16 demonstrate this fact. The temperature distributions along the nozzle wall are given in Fig. 17. When the particle mass fraction is increased, the high temperature is observed, and the peak value becomes large.

Conclusions

By regarding the particles as sources of mass, momentum, and energy, the trajectory model has been applied to the solid rocket nozzle flow. Because the phase change of particles is neglected in this study, the particle mass source becomes zero. A time-dependent, explicit MacCormack scheme was used to solve the Navier-Stokes equations with/without particle effects. The velocity, position, and temperature of particles are calculated by the Lagrangian approach. To study the mutual interactions between gas and particle phases, the empiricisms, such as drag coefficient and Nusselt number, are incorporated into the trajectory model. For the inviscid gas-particle flow, the predicted physical phenomena are consistent with those of the two-fluid model. In order to understand the turbulent effect on particle dispersion, the diffusive velocity of the particle is calculated. Compared with the convective velocity, the values of diffusive velocity are very small for the present model.[11,13,15,20] For the viscous gas-particle flow, the peak values of gas temperature appear on the nozzle wall around the particle separation points. The magnitudes of these peak values become large when the two-phase flows include small sizes and high mass fractions of particles. From the results of this paper and Ref. 7, it is observed that the convergence of solutions for the two-phase flows with small particles is slow when the trajectory model is applied. The special numerical treatments, however, are required when the two-fluid model is introduced to solve the gas-particle flows with large particle sizes. The range of applicability, advantages and disadvantages of the two-fluid and trajectory models were discussed by Crowe.[4,21]

References

[1]Hoglund, R. F., "Recent Advances in Gas-Particle Nozzle Flows," *ARS Journal*, Vol. 32, May 1962, p. 662.

[2]Kliegel, J. R., "One Dimensional Flow of a Gas Particle System," TR-59-0000-00746, Space Technology Laboratory, July 1959.

[3]Kliegel, J. R. and Nickerson, G. R., "Flow of Gas-Particle Mixtures in Axially Symmetric Nozzles," *Progress in Astronautics and Rocketry*, Vol. 6, Academic Press, New York, 1962, pp. 173–194.

[4]Crowe, C. T., "Review—Numerical Models for Dilute Gas-Particle Flows," *Journal of Fluids Engineering*, Vol. 104, Sept. 1982, pp. 297–303.

[5]Nickerson, G. R., Coats, D. E., and Hermsen, R. W., "A Computer Program for the Prediction of Solid Propellant Rocket Motor Performance," AFRPL-TR-80-34, Vol. I, June 1980.

[6]Chang, I-Shih, "One- and Two-Phase Nozzle Flows," AIAA Paper 80-0272, Jan. 1980.

[7]Hwang, C. J., "A Theoretical Study of Compressible Two Phase Internal Flow," Ph.D. Dissertation, Univ. of Tennessee Space Institute, Aug. 1984.

[8]DiGiacinto, M., Sabetta, F., and Piva, R., "Two-Way Coupling Effects in Dilute Gas-Particle Flows," *Journal of Fluids Engineering*, Vol. 104, Sept. 1982, pp. 304–312.

[9]Crowe, C. T., Sharma, M. P., and Stock, D. E., "The Particle-Source—In Cell (PSI-CELL) Model for Gas-Droplet Flows," *Journal of Fluids Engineering*, Vol. 99, June 1977, pp. 325–332.

[10]Dukowicz, J. K., "A Particle-Fluid Numerical Model for Liquid Sprays," *Journal of Computational Physics*, Vol. 35, April 1980, pp. 229–253.

[11]Melville, E. K. and Bray, N. C., "A Model of the Two-Phase Turbulent Jet," *International Journal of Heat and Mass Transfer*, Vol. 22, May 1979, pp. 647–656.

[12]Cline, M. C., "VNAP2: A Computer Program for Computation of Two-Dimensional, Time-Dependent, Compressible, Turbulent Flow," LA-8872, Los Alamos National Laboratory, 1981.

[13]Jones, W. P. and Launder, B. E., "The Prediction of Laminarization with a Two-Equation Model of Turbulence," *International Journal of Heat and Mass Transfer*, Vol. 15, Feb. 1972, p. 301.

[14]Elghobashi, S. E. and Abou-Arab, T. W., "A Two-Equation Turbulence Model for Two-Phase Flows," *Physics of Fluids*, Vol. 26, April 1983, pp. 931–938.

[15]Smith, P. J. and Smoot, L. D., "Combustion Processes in a Pulverized-Coal Combustor," EPRI CS-2490-CCM, July 1982.

[16]Weast, R. C., Astle, M. J., and Beyer, W. H., *Handbook of Chemistry and Physics*, 65th ed., CRC, FL, 1984–1985, p. D-43.

[17]Schaff, S. and Chambre, P., "Flow of Rarefied Gases," *Fundamentals of Gas Dynamics*, Princeton Series, Vol. III, Princeton Univ., 1958, p. 725.

[18]MacCormack, R. W., "The Effect of Viscosity in Hyper-Velocity Impact Cratering," AIAA Paper 69-354, April 1969.

[19]Patankar, S. V., "Convection and Diffusion," *Numerical Heat Transfer and Fluid Flow*, Hemisphere, New York, 1980, pp. 79–111.

[20]Branch, M. C., "Flow of Gas-Particle Mixtures," AFOSR-TR-83-0272, Nov. 1982.

[21]Crowe, C. T., "Two-Fluid vs. Trajectory Models: Range of Applicability," ASME Paper, FED-Vol. 35, May 1986, pp. 91–95.